Feasibility of MRI-only treatment planning for proton therapy in brain and prostate cancers: Dose calculation accuracy in substitute CT images

Lauri Koivula[a)]
Department of Radiation Oncology, Comprehensive Cancer Center, Helsinki University Central Hospital, P.O. Box 180, Helsinki 00029 HUS, Finland and Department of Medical Physics, Oncology Services, Vejle Hospital, Kabbeltoft 25, Vejle DK-7100, Denmark

Leonard Wee
Department of Medical Physics, Oncology Services, Vejle Hospital, Kabbeltoft 25, Vejle DK-7100, Denmark and Danish Colorectal Cancer Centre South, Vejle Hospital, Kabbeltoft 25, Vejle DK-7100, Denmark

Juha Korhonen
Department of Radiation Oncology, Comprehensive Cancer Center, Helsinki University Central Hospital, P.O. Box 180, Helsinki 00029 HUS, Finland; Danish Colorectal Cancer Centre South, Vejle Hospital, Kabbeltoft 25, Vejle DK-7100, Denmark; and Department of Radiology, Helsinki University Central Hospital, P.O. Box 180, Helsinki 00029 HUS, Finland

(Received 9 March 2016; revised 29 May 2016; accepted for publication 29 June 2016; published 18 July 2016)

Purpose: Magnetic resonance imaging (MRI) is increasingly used for radiotherapy target delineation, image guidance, and treatment response monitoring. Recent studies have shown that an entire external x-ray radiotherapy treatment planning (RTP) workflow for brain tumor or prostate cancer patients based only on MRI reference images is feasible. This study aims to show that a MRI-only based RTP workflow is also feasible for proton beam therapy plans generated in MRI-based substitute computed tomography (sCT) images of the head and the pelvis.
Methods: The sCTs were constructed for ten prostate cancer and ten brain tumor patients primarily by transforming the intensity values of in-phase MR images to Hounsfield units (HUs) with a dual model HU conversion technique to enable heterogeneous tissue representation. HU conversion models for the pelvis were adopted from previous studies, further extended in this study also for head MRI by generating anatomical site-specific conversion models (a new training data set of ten other brain patients). This study also evaluated two other types of simplified sCT: dual bulk density (for bone and water) and homogeneous (water only). For every clinical case, intensity modulated proton therapy (IMPT) plans robustly optimized in standard planning CTs were calculated in sCT for evaluation, and vice versa. Overall dose agreement was evaluated using dose–volume histogram parameters and 3D gamma criteria.
Results: In heterogeneous sCTs, the mean absolute errors in HUs were 34 (soft tissues: 13, bones: 92) and 42 (soft tissues: 9, bones: 97) in the head and in the pelvis, respectively. The maximum absolute dose differences relative to CT in the brain tumor clinical target volume (CTV) were 1.4% for heterogeneous sCT, 1.8% for dual bulk sCT, and 8.9% for homogenous sCT. The corresponding maximum differences in the prostate CTV were 0.6%, 1.2%, and 3.6%, respectively. The percentages of dose points in the head and pelvis passing 1% and 1 mm gamma index criteria were over 91%, 85%, and 38% with heterogeneous, dual bulk, and homogeneous sCTs, respectively. There were no significant changes to gamma index pass rates for IMPT plans first optimized in CT and then calculated in heterogeneous sCT versus IMPT plans first optimized in heterogeneous sCT and then calculated on standard CT.
Conclusions: This study demonstrates that proton therapy dose calculations on heterogeneous sCTs are in good agreement with plans generated with standard planning CT. An MRI-only based RTP workflow is feasible in IMPT for brain tumors and prostate cancers. [http://dx.doi.org/10.1118/1.4958677]

Key words: MRI-only, radiotherapy treatment planning, substitute CT image, intensity modulated proton therapy, Hounsfield unit conversion

1. INTRODUCTION

Magnetic resonance imaging (MRI)-based contouring is presently standard practice in radiotherapy.[1–4] Recently, the use of MR images has been extended for the entire external photon radiotherapy treatment planning workflow.[5–18] The development of techniques that construct electron density in MRI-derived substitute computed tomography images (sCT,

also known as pseudo CT, synthetic CT or virtual CT) has been an essential milestone enabling omission of CT from the workflow.[5–7,9,10,12–16,19] Previous work in photon treatment planning has shown that absorbed dose can be accurately computed in sCT, and these images can also be applied as reference images for image-guided radiotherapy (IGRT) with x-ray-based localization.[5–10,12,14,15,17,18] Clinical interest in MRI localization-based IGRT has been growing in recent years due to developments in MRI-guided radiotherapy, such as MR-linacs, MR-on-rails, and table-trolley systems.[20–24] Volumetric MR studies are also increasingly utilized for post-treatment monitoring.[25–27]

High quality soft-tissue visualization in MRI assists target delineation and image guidance needed for intensity modulated proton therapy (IMPT) to realize its maximum clinical potential for avoiding radiation toxicity.[28–31] Furthermore, an MRI-only based planning process avoids MR-to-CT registration uncertainties, minimizes radiation toxicity, and saves hospital resources.[5–10,12–16,18] Online IMPT planning on the basis of MR localization imaging would be of major importance for MR-proton radiotherapy systems that may appear in future.[31,32]

The feasibility of MRI-only based planning for particle beam therapy has been tested previously by Edmund *et al.*[14] and Rank *et al.*[33,34] Both works employed ultrashort echo time (UTE) sequence-based sCT construction methods for the head and reported approximately 2% dose calculation accuracy in sCT compared to CT. Edmund *et al.* conducted dose calculations in several different types of sCT for uniform scanning proton beams in five patients with simulated spherical tumor targets placed between the nasal cavity and skull. In the best performing sCT, the mean absolute error (MAE) of Hounsfield units (HUs) was 128. Rank *et al.* calculated proton and carbon ion plans for three brain tumor cases using an in-house treatment planning system.[33,34] The MAE of HU in their case was 149.

Hartman *et al.* recently showed that a 0.6 T magnetic field directed transverse to a proton beam during irradiation affects the selection of IMPT spot positions due to Lorentz-force deflection of the protons in air, but does not significantly disturb the dose distribution around the target.[35] Field-induced deflection corrections are not relevant for offline MRI, post-treatment MRI, charged particles travelling parallel to a magnetic field,[32] or if an MR-on-rails design is employed.[23]

In this paper, we focus specifically on evaluating dose calculation accuracy for robustly optimized IMPT with MRI-derived planning sCTs for a validation cohort of ten brain tumor cases and ten prostate cancer cases. Our work addresses dose uncertainties in IMPT plans arising from three types of sCTs: (1) homogeneous, (2) dual bulk, and (3) heterogeneous density conversion.[5–9,36] We compare the dose calculation accuracy when performing robust IMPT plan optimization in the CT followed by dose computation in sCT and vice versa.

2. METHODS

2.A. Construction of substitute CTs

The feasibility of MRI-only based planning with protons was validated using 20 entirely different test cases (10 brain tumors and 10 prostate patients) with three sCT generation methods for use in IMPT: (1) assigning the entire body volume to water-equivalent density (homogeneous), (2) setting an average bulk density for bone and water-equivalent density to the rest of the body (dual bulk), and (3) transforming the voxel intensities of an in-phase MR image to HU by a dual model conversion technique (heterogeneous). The latter applies separate density conversion models for bone and soft tissue after autocontouring bone outlines.[5–7,9] The technique has been used to generate heterogeneous sCTs of the pelvis, and it is presently used in routine clinical external photon MRI-only planning workflow for prostate cancer.[4–7,9] In the current study, this dual model HU conversion technique was also extended to the head.

Imaging was performed according to our department's (Helsinki, Finland) standard procedures for MRI + CT-based radiotherapy treatment planning (RTP) for both prostate and brain tumor patients. Prostate patients undergoing MRI-only based RTP protocol in our clinic were excluded from this specific study because their simulation protocol does not include CT scanning. Both MRI and CT simulations (MR simulator: 1.5 T imager GE Optima MR450w, GE Medical Systems, Inc., Waukesha, WI, USA. CT simulators: either GE LightSpeed RT, GE Medical Systems, Inc., or Siemens SOMATOM Definition AS, Siemens Healthcare, Erlangen, Germany) were conducted with patient positioning similar to that for treatment. The MR scanner was equipped with accessories such as laser-localization system, flat table top, MR compatible fixation devices, and receiver coil frames.[6,9,11] In-phase MR images obtained by a T1/T2*-weighted 3D fast RF-spoiled dual gradient echo sequence were used to create sCT because previous work had shown that accurate heterogeneous sCT of the pelvis are obtained.[6–9,11,36] Our department's standard simulation procedures for RTP already contains the above dual echo sequence among a set of MR examinations used mainly for target delineation. The same imaging protocol was retained for the current study. The specific sequence parameters for in-phase images were as follows: TE = 4.2 ms, TR = 6.8 ms, flip angle = 15°, and bandwidth = 90.9 kHz (pelvis) or 62.5 kHz (head) with approximate scan times of 2 and 3 min for the head and pelvis, respectively. The applied standard MRI sequence does not permit differentiation of cortical bone and air cavities (where UTE sequences are required).[6,7,9,13,37] This differentiation is not required if treatment fields do not pass through air cavities, that would typically be the case with proton beam therapy for brain tumors.[38–40] The system-related geometrical uncertainties in the applied MR images remain within 1 mm [field-of-view (FOV): 24 cm] in the head and within 2 mm (FOV: 42 cm) in the pelvis.[5,9,11] The susceptibility-induced shifts of tissue boundaries remain within 1 mm (soft tissue-bone) and 2 mm (soft tissue-air, mean body outline error of 1.2 mm in pelvis).[9,11] Although the entire MRI simulation protocol included other sequences, the other images were not used in this study. The imaging time for all sequences in the current simulation protocol was about 12 and 20 min for the head and the pelvis, respectively. The voxel size used in the MR and CT images was about 1 mm^3.

The heterogeneous sCTs for ten prostate cancer patients were obtained by following the clinical MRI-only planning workflow, in which the bone contouring and density conversion are integrated into a commercial image processing software MIM VISTA v5.6 (MIM Software, Inc., Cleveland, OH, USA).[4–9] The heterogeneous sCTs for ten brain tumor patients were achieved by further extending the conversion technique to the head. The conversion models were adjusted particularly for this body site by using volume-of-interest (VOI)-based correspondence between the MR intensities and CT HUs from imaging data of ten other patients in the same setup.[5,6,9] In total, 700 VOIs (2 mm diameter, 4 mm^3, 70 VOIs/patient) were placed in different soft tissues and bones in the MR image of the head (such as white matter, gray matter, cerebrospinal fluid, cortical bone, and spongy bone). The MR image was rigidly coregistered to the CT using the mutual information method in MIM VISTA, and the average HU and MR intensities in each VOI were recorded as paired values.

The sampled-VOI data were used to create HU conversion models separately within and outside of a bone segment. In bone, the conversion model was an exponential fit to the data. In soft tissue, the conversion model was a piecewise function that segregates fluid, white matter, gray matter, and scalp according to the mean and standard deviation of MR intensities for particular tissue type. For each tissue type, an appropriate average HU was assigned.[41–44] Potential gaps in the MR intensity scale between tissues were bridged by linear interpolation.

The resulting conversion models were integrated into a commercial medical image processing software (MIM VISTA). Conversion time from MR image to the sCT was approximately 30 s per patient with Intel Xeon quad-core (3.07 GHz) processor accompanied by 12 GB of RAM. For validation, the technique was applied for the ten different brain tumor patients (precise manual bone contouring followed by the autotransformation of MR intensities into HUs). The HU accuracy in the resulting sCTs was analyzed by HU value comparison against CT images using the same VOI-based sampling as for generating the models.

2.B. Treatment planning

IMPT plans for ten prostate and ten brain treatments were produced on a stand-alone PC using RAYSTATION v4.7.2 treatment planning software (Raysearch Laboratories, Stockholm, Sweden) and a generic scanned pencil beam model for a compact single-gantry proton delivery system. Clinically feasible plans were produced using a standard snout (10 cm) and standard range shifters (0, 4.5, and 7 cm). Minimum spot weights were fixed at 0.01 monitor units per fraction, but there were no explicit restrictions for spot arrangement or number of energy layers. Couch rotation in each plan was fixed at 0°. Treatment plan isocenters for brain treatments were placed at the midsagittal plane and on the transverse slice containing the center of mass of the planning target volume (PTV); however, the anterior–posterior (AP) placement was individually adapted in each plan. Treatment plan isocenters for prostate treatments were always located at the center of mass of the clinical target volume (CTV).

Dose to the CTV was inverse-planned with robust optimization with respect to localization perturbation and range uncertainty.[45] Surrounding dose fall-off and maximum dose–volume histogram (DVH) objective functions were used to minimize dose outside the CTV. Each plan was first optimized and computed on CT, and then only dose was computed in each type of sCT. This validated the accuracy of dose calculation in an sCT relative to the CT. To examine the effect of sCT on plan optimization, we made fresh optimizations first in each sCT and then computed dose only in the CT. Only for the purpose of accurately testing dose discrepancies within the body arising mainly due to sCT density assignment, we removed the effect of patient misalignment between CT and MRI scans by using an identical external skin outline in both sCT and CT. The skin outline in the CT was copied to the MRI, but only tissue voxels in the MRI overlapping with the CT were used to generate the sCT.[3,5,9] Possible complement volume between CT and MRI skin contours (CT \ MRI) was set to water equivalent. In an MRI-only clinical workflow, this step is not required since the sCT conversion will involve the entire patient outline found in the MRI scan.

For robust optimization using the worst-case method,[45] we applied spatial offsets of 1, 2, and 3 mm in each cardinal direction, due to uncertainties from beam modeling, organ delineation and residual errors in patient localization. Beam range uncertainty was simulated in the robustness optimization by uniformly scaling all physical density values up and down by 3%, with and without the spatial perturbation.

A template-based approach was used for prostate plans with bilateral beams at constant gantry angles of 90° and 270°, and no range shifter. Final dose was calculated on a 2 mm isotropic grid and rescaled such that 2.2 Gy [relative biological effectiveness (RBE)] dose per fraction was always prescribed to 98% of PTV.

A wide range of tumor volumes and locations required an individually customised approach for brain IMPT beam placement. One or two beams were positioned to avoid the eyes, brainstem, and air cavities. The plans sampled a wide variety of different gantry angles, range shifters, and isocenter placements. Final dose was calculated on a 1 mm isotropic grid and rescaled for 2.2 Gy (RBE) per fraction prescribed to 95% of CTV.

For planned and evaluation dose analysis, the entire dose grid covering all targets and organs at risk was extracted with PYTHON scripting for gamma analysis. Gamma index "pass" rates were calculated over dose grid points in sCT with 10% of the prescribed dose or higher, for several dose and distance criteria, compared to the dose calculated in CT. DVH statistics were obtained from the plan printouts. For wider generalizability, we also compared CT versus sCT dose calculation accuracy in IMPT to volumetric modulated arc therapy (VMAT) using 6 MV photons.

3. RESULTS

3.A. Heterogeneous substitute CTs

Table I shows the HU conversion models used in the head scans to transform in-phase MR images into sCTs. Figures 1

TABLE I. The dual conversion models for the head to transform in-phase MR image intensity values into HUs separately for bone and soft tissue.

Tissue type	MR intensity (x)	HU	Details
Bone	$x < 200$	1441	Cortical bone
	$200 \le x \le 2000$	$e^{7.42-0.001x+1.3\times10^{-7}x^2}$	Mixed bone tissues
	$x > 2000$	360	Spongy bone
Soft tissue	$x < 338$	12	Fluid
	$338 \le x < 576$	From 12 to 45[a]	Boundaries and noise
	$576 \le x < 798$	45	Gray matter
	$798 \le x < 1060$	25	White matter
	$1060 \le x < 2285$	From 25 to −83[a]	Boundaries and noise
	$x > 2285$	−83	Scalp

[a]The MR intensities were transformed into HUs with linear interpolation.

and 2 illustrate examples of heterogeneous sCTs of the head and the pelvis, respectively, shown with display window levels for soft tissue and bone. All heterogeneous sCTs reliably reproduced the qualitative appearance of different tissue types found in the head and pelvis as in CT. The overall HU MAE in heterogeneous head sCTs was 34 HU (13 HU in soft tissue, 92 HU in bone). These uncertainties were comparable to the overall MAE in heterogeneous pelvic sCTs of 42 HU (9 HU in soft tissue, 97 HU in bone).

3.B. Dose calculation accuracy in substitute CTs

The distributions of DVH differences between sCTs and CTs were summarized in box-and-whisker plots for the ten brain cases (Fig. 3, omitting the homogeneous sCT) and for the ten prostate cases (Fig. 4). The relative cumulative volume of a target or risk organ has been plotted on the horizontal axis, and the percentage dose difference in sCT relative to CT has been plotted on the vertical axis. The mean CTV dose differences between heterogeneous sCTs and CTs were −0.2% (range: −1.4%–0.9%) and 0.1% (range: −0.5%–0.6%) for the ten brain tumor and ten prostate cancer patients, respectively. The corresponding dose differences in dual bulk sCTs were 0.1% (range: −1.4%–1.8%) and −0.3% (range: −1.2%–0.8%), respectively. Larger CTV dose differences were observed for homogenous sCT both in head (mean: −1.6%, range: −8.9%–2.3%) and in pelvis (mean: 0.7%, range: −3.6%–2.4%).

For whole brain DVHs [Fig. 3(B)], the mean difference (and range) in calculated dose from CT was −0.1% (−1.1%–2.6%), 0.1% (−1.2%–0.7%), and 1.5% (−2.8%–13.8%) for heterogeneous, dual bulk, and homogeneous sCTs, respectively. In rectal DVHs, mean sCT differences were within 0.1% of CT and worst differences were within 1.8% in all cases. In bladder DVHs, heterogeneous sCTs performed well in all cases (mean: 0.0%, range: −0.4%–0.9%), but there were differences up to 3% in dual bulk sCT (mean: −0.4%, range: −3.1% to 0.8) and up to 10% in homogeneous sCT (mean: 0.3%, range: −2.2%–10.2%).

Table II presents the gamma index evaluations for IMPT plans between CT and sCT for every dose point over 10% of the prescribed dose. With the heterogeneous sCTs of both pelvis and brain, the mean pass rate for the 1% and 1 mm gamma index criterion was over 95% (worst cases: 92.4% in pelvis and 90.5% in head). Dual bulk sCTs had mean pass rates over 95% for the 2% and 2 mm criterion. The homogeneous sCT did not reach average pass rates over 95% even with 3% and 3 mm gamma index criterion.

A further consideration for IMPT planning is whether the use of a sCT during robust optimization has any effect on dose calculation accuracy relative to CT. Ideally, the dose calculation accuracy should remain the same with respect to interchanging the image sets used for inverse-planning and dose calculation. Figure 5 presents the gamma index for each plan created using a sCT and then evaluated for dose calculation in CT, plotted as a function of its corresponding CT-planned and sCT-evaluated gamma index.

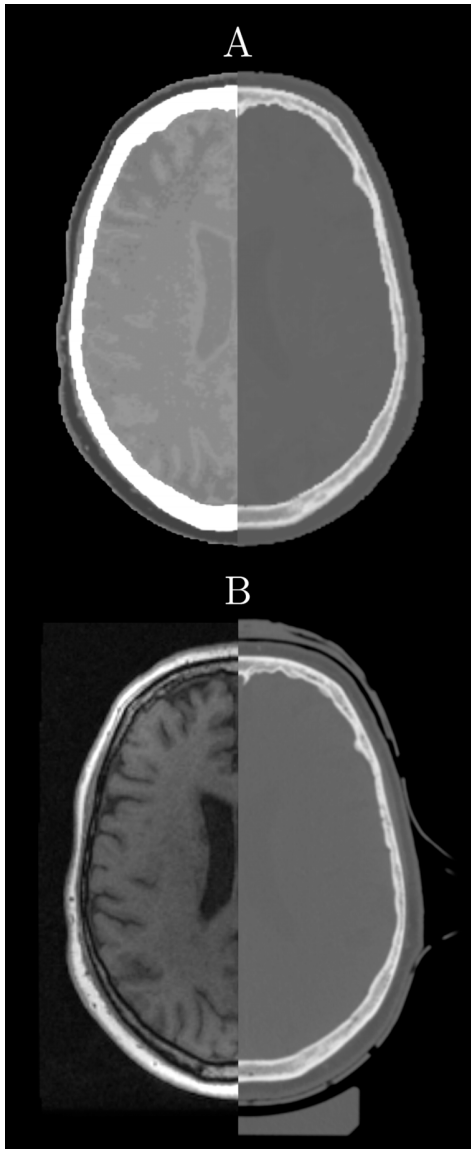

FIG. 1. An example of a heterogeneous sCT of the head in (A) displayed with soft tissue window (left) and bone window (right). The original MR in-phase image is shown in (B) on the left and the standard planning CT in (B) on the right.

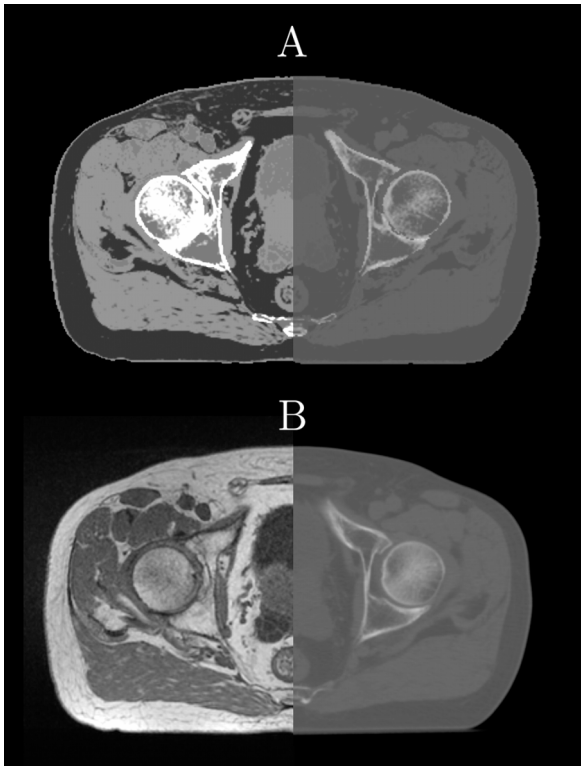

FIG. 2. An example of a heterogeneous sCT of the pelvis in (A) displayed with soft tissue window (left) and bone window (right). The original in-phase MR image is shown in (B) on the left and the standard planning CT in (B) on the right.

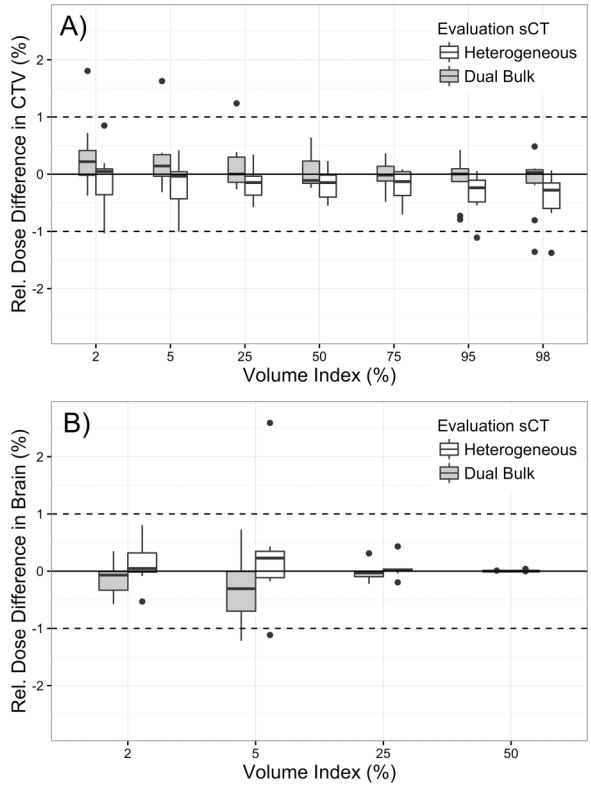

FIG. 3. Differences in dose (reference planning data was actual CT, then IMPT doses were calculated in heterogeneous and dual bulk sCTs) at a given cumulative relative volume for the (A) CTV and (B) whole brain. The dashed lines indicate the ±1% relative dose difference in sCT compared to dose calculated in actual CT. The results for CTV and whole brain DVHs in the homogeneous sCT were ranging up to 8.9% and to 13.8%, respectively. These have been omitted from the figure to preserve visual clarity.

The photon dose calculation results followed roughly the same pattern of agreement as with protons. Mean prostate PTV dose differences in calculated VMAT photon plans between sCTs and CTs were −0.1% (range: −0.5%–0.3%), 0.4% (range: −0.4%–1.0%) and −1.2% (range: −2.2%–0%) for heterogeneous, dual bulk, and homogeneous sCTs, respectively. The corresponding evaluations for brain PTV dose differences were −0.1% (range: −0.4%–0.7%), 0.3% (range: −0.1%–0.9%), and −2.7% (range: −3.9 to −1.0).

4. DISCUSSION

The current standard for proton treatment planning is the dose distribution calculated on a CT obtained during simulation. We herein show that it is feasible to calculate proton dose on sCT derived solely from MR images, such that a given planned distribution of spots (and spot weights) yields dose distributions that are in close agreement to those in CT image sets. The dose calculations in different type of sCTs illustrate the influence of heterogeneity to the dose agreement. For targets in the head and pelvis, dose differences from heterogeneous sCT to CT were mainly within 0.5%. Also gamma indices were satisfactory for both targets and healthy tissues, even for 1% and 1 mm criteria. The dose calculation uncertainty due to heterogeneous sCT construction is therefore comparable or minor in magnitude to potential uncertainties caused by CT-to-density calibration uncertainties, anatomical changes in the patient, and IGRT localization errors.[46–48]

In addition to heterogeneous tissue presentation, the dual bulk sCTs performed well reaching IMPT dose calculation accuracy better than 2% for all cases. The fully homogeneous sCTs introduced unacceptable dose errors for some patients. Hence, the use of sCTs including at least separate bulk densities for bones and soft tissues is essential, while increasing heterogeneity further provides higher dose accuracy and reliability for all patients. With heterogeneous and dual bulk sCTs, the proton dose calculation uncertainty was nearly in a comparable level with external photon MRI-only based planning.

The good performance of dual bulk sCT may have stemmed from the selected beam directions. The beams had been directed mostly through bones having relatively homogeneous composition (e.g., femoral heads and skull). If beams pass through bones with a dense shell of cortical bone covering less-dense bone marrow (e.g., femur, ilium, and pubic bone), then the heterogeneous tissue presentation in sCTs appears to be essential for accurate dose calculation.[36] In head and neck cases, where the treatment beams must be directed through air cavities, an accurate heterogeneous sCTs would be mandatory. If the tumor is located in a close proximity to nasal cavities or when applying beams from the anterior direction, accurate representation of bone structure, cartilage, and air cavities is essential. In such cases, a clinical user should use either UTE

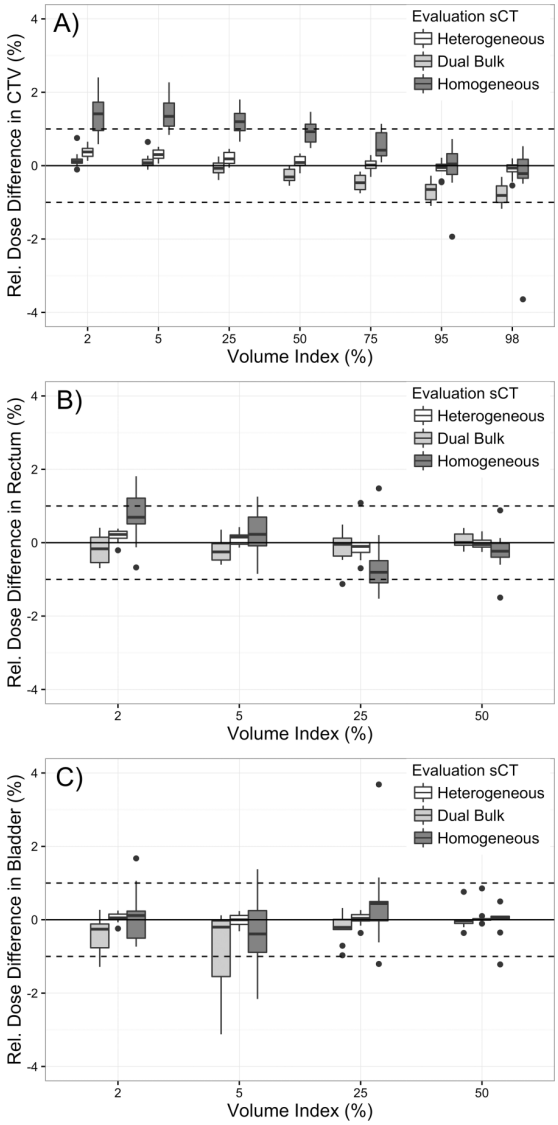

FIG. 4. Differences in dose (reference planning data was actual CT, then IMPT doses were calculated in heterogeneous and dual bulk sCTs) at a given cumulative relative volume for the (A) prostate CTV, (B) rectum, and (C) bladder. Dashed lines indicate the ±1% relative dose difference compared to dose calculated in actual CT.

sequence-based or atlas-based approaches for sCT generation. However, accurate representation of air-bone interfaces could be challenging even with those sCT construction methods that might be a reason for higher HU uncertainty for the head in previous studies (MAE: 126–149) compared to the present work excluding air cavity volumes (MAE: 34).[13,14,19,33] In the conversion-based heterogeneous sCTs of the pelvis, the HU MAE was similar (whole pelvis: 42, bones only: 97) to that reported previously (whole pelvis: 37–74, only bones: 98–134).[5,9,12,49,50] Earlier studies have shown that various types of heterogeneous pelvic sCTs perform dosimetrically acceptably for dose calculation with photons. According to the current study, heterogeneous sCTs are also acceptable for IMPT planning.[12–14,17,49,50]

The heterogeneous sCT generation method used in the current study relies on bone segmentation of the MR image, before performing the distinct MR intensity to HU conversion within and outside of the segment. Our method was designed to be highly accessible and easily adopted by most clinical users, but the method commissioning has some limitations. Every user needs to commission and validate a suitable bone segmentation algorithm. Due to the straightforward direct conversion process, conversion models should be revalidated in case of any changes in the MR platform or acquisition that leads to changes in MR absolute intensities or in the image uniformity.[5,9,11] The method is robust for general changes in MR intensity levels and in the absence of major artifacts.

Intrafraction uncertainties would still need to be accounted for using adequate margins or adopting a target motion-following approach. The latter is an appealing future application of MR-guidance during beam delivery. With this conversion method it is possible to generate an sCT rapidly (within 30 s) but the time required for autosegmentation and treatment plan optimization remain the limiting steps. However, our method would be readily compatible with future advances in online adaptive replanning that could address some of these computational issues.

Although a large number of details could be examined in regards to plan quality, this study design focused only on the potential dose calculation errors arising due to use of sCT, relative to CT-simulation. Our beam arrangements in the head were designed to avoid treatment through air cavities. In prostate cases, air pockets in the lower bowel were occasionally unavoidable. The sCT generation methods above had assigned bowel gas as water-equivalent.[6] This led to an additional contribution to the observed dose differences in the prostate plans. The use of a matching skin contour between sCT and CT, as we have described above, was considered as the best solution to avoid dose comparison

TABLE II. The percentages of dose points of IMPT plans in sCTs compared to those in CTs that passed the 3D gamma index criteria are presented as averages (and range) of ten patients each in the pelvis and in the head.

		3D gamma index criteria		
		3% & 3 mm	2% & 2 mm	1% & 1 mm
Pelvis	Heterogeneous	99.6 (99.0–100)	98.6 (97.2–99.9)	95.0 (92.4–98.2)
	Dual bulk	98.8 (97.2–99.8)	97.2 (95.0–99.4)	92.6 (89.6–95.8)
	Homogeneous	90.7 (87.5–94.5)	86.8 (83.0–91.0)	78.7 (74.0–83.8)
Head	Heterogeneous	99.9 (99.8–100)	99.5 (98.0–100)	95.9 (90.5–100)
	Dual bulk	99.9 (99.1–100)	99.3 (96.6–100)	94.3 (85.1–99.9)
	Homogeneous	84.1 (76.0–98.2)	71.5 (57.9–80.4)	53.6 (38.4–63.2)

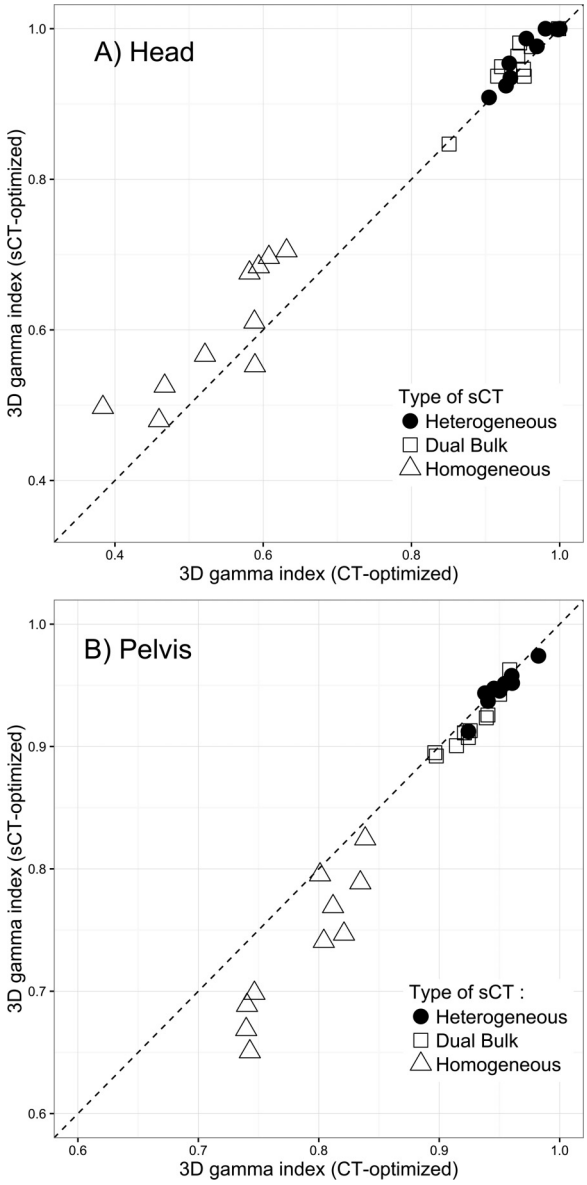

FIG. 5. The effect on dose calculation agreement due to the image type used for inverse planning is shown for IMPT plans in the (A) head and (B) pelvis. The horizontal axis gives gamma indices for plans created using CT and then evaluated for dose calculation accuracy in different types of sCT. The vertical axis gives corresponding gamma indices for plans created with an sCT then evaluated in the CT. The locus of points which are invariant with respect to interchanging image sets are plotted as a dashed line as an aid for the eye.

uncertainties stemming from patient body outline changes observed between MR and CT scans. Automated deformable registration was considered as an option to avoid the need for manual correction of the skin contour, but that would have introduced additional registration-related uncertainties for internal organs. With manual correction of the air-skin interface, it was mainly the internal changes of organs (e.g., rectal gas) between CT and MR simulation that would have contributed to the dose differences in addition to the intrinsic quality of sCT construction. The change in bladder filling was minimal as scans were acquired one following the other as a part of the routine clinical RTP simulation workflow.

Robustness is presently considered a standard requirement for proton therapy planning, so we have incorporated robust optimization in all of our IMPT plans.[51–55] Our robustness settings assume that any systematic and random shift in the target position will be accounted for using daily online imaging and position correction; this would be reasonable for proton therapy given recent developments in IGRT.[56–58] Robustness settings would have no impact on the average dose agreement between heterogeneous sCT and CT. Different perturbation distances might shift the observed gamma pass rates for homogeneous sCT and dual bulk sCT relative to the (dotted) line of equivalence on Fig. 5.

Some studies have pointed out uncertainties in the stopping power ratios for protons used in the dose computation.[59–61] Our findings remain unchanged because our dose calculations used a fixed relationship between physical density and stopping powers for all image sets. We have used 3% scaling of physical density in robust optimization to allow for potential errors in the stopping power ratios. During robust optimization, the dose calculation accuracy relative to CT was unaffected by using the heterogeneous sCT, and only minimally using the dual bulk sCT. Fully homogeneous sCT performed poorly for accuracy relative to CT when used for the optimization. In Fig. 5(A), with homogeneous sCT there is a general tendency for the points to lie above and to the left of the line of invariance. In Fig. 5(B), the tendency instead is for the points to lie below and to the right of the dashed line. In the head, there is a relatively little density variation within brain tissue, and the cranium is approximately a uniform spherical shell of cortical bone overshadowing the target volume. Plans optimized first in the sCT are less sensitive to internal density variations but are affected by patient shape, and hence return higher gamma pass rates compared to plans optimized first in the CT. In the pelvis, the bones are irregular in shape and provide differential shielding of the target when viewed along the beam axis. The bone density structure is also more complex, being a composite of bone marrow, spongy bone and cortical bone. Plans optimized first in the homogeneous sCT do not adequately account for changes in both shape and physical density, and hence can return lower pass rates compared to plans optimized first in the CT. We propose that the effect of using sCT in different robust optimization approaches would be an interesting subject for further study. The body of published work on MRI-only based treatment planning for proton therapy suggests that this is a promising area of future clinical utility; therefore, further publications on this subject would be warranted for pediatric proton therapy or address treatment sites other than brain and prostate.

5. CONCLUSIONS

This study shows that proton dose calculation can be performed accurately in MRI-derived sCT images for brain tumor and prostate cancer cases. Overall, proton dose computation in sCT images was marginally more accurate in prostate plans than for brain plans. Heterogeneous sCTs achieved dose agreement of approximately 1% or better for target volumes and organs at risk for all patients both in head and pelvis

regions. Dose agreement compared with CT was unaffected by robust optimization when using the heterogeneous sCT as the planning image set. Robust optimization can also be reliably performed in heterogeneous sCTs wherein the patient's shape and density variations have been reproduced with high fidelity. Dual bulk sCTs also attained 1% level of dose agreement for many patients, but showed larger variability in dose uncertainties regarding the entire patient groups, and included also higher risk for dose errors in small volumes of targets and healthy organs. However, the dose accuracy remained sufficient, and thus the dual bulk sCTs could also be considered for clinical applications if heterogeneous sCTs are unavailable. Fully homogenous density substitution cannot be recommended in any case.

ACKNOWLEDGMENTS

The authors acknowledge the valuable work of Mikko Tenhunen, Mika Kapanen, Tiina Seppälä, Harri Visapää, Kauko Saarilahti, and others from the Comprehensive Cancer Center of Helsinki (Finland) for MRI-only based planning. The authors also acknowledge assistance from the Oncology Department of Vejle Hospital (Denmark), the Danish Colorectal Cancer Centre South and RaySearch Laboratories (Sweden).

CONFLICT OF INTEREST DISCLOSURE

The authors have no COI to report.

[a]Electronic mail: lauri.koivula@helsinki.fi

[1]V. S. Khoo and D. L. Joon, "New developments in MRI for target volume delineation in radiotherapy," Br. J. Radiol. **79**(Spec No 1), 2–15 (2006).
[2]A. Sciarra, J. Barentsz, A. Bjartell, J. Eastham, H. Hricak, V. Panebianco, and J. A. Witjes, "Advances in magnetic resonance imaging: How they are changing the management of prostate cancer," Eur. Urol. **59**(6), 962–977 (2011).
[3]P. Dirix, K. Haustermans, and V. Vandecaveye, "The value of magnetic resonance imaging for radiotherapy planning," Semin. Radiat. Oncol. **24**(3), 151–159 (2014).
[4]T. Seppala, H. Visapaa, J. Collan, M. Kapanen, A. Beule, M. Kouri, M. Tenhunen, and K. Saarilahti, "Converting from CT- to MRI only-based target definition in radiotherapy of localized prostate cancer: A comparison between two modalities," Strahlenther. Onkol. **191**(11), 862–868 (2015).
[5]L. Koivula, "Magnetic resonance imaging- based radiation therapy treatment planning," Master's thesis, University of Helsinki, 2016, pp. 1–38.
[6]J. Korhonen, M. Kapanen, J. Keyrilainen, T. Seppala, and M. Tenhunen, "A dual model HU conversion from MRI intensity values within and outside of bone segment for MRI-based radiotherapy treatment planning of prostate cancer," Med. Phys. **41**(1), 011704 (64pp.) (2014).
[7]J. Korhonen, M. Kapanen, J. Keyrilainen, T. Seppala, L. Tuomikoski, and M. Tenhunen, "Influence of MRI-based bone outline definition errors on external radiotherapy dose calculation accuracy in heterogeneous pseudo-CT images of prostate cancer patients," Acta Oncol. **53**(8), 1100–1106 (2014).
[8]J. Korhonen, M. Kapanen, J. J. Sonke, L. Wee, E. Salli, J. Keyrilainen, T. Seppala, and M. Tenhunen, "Feasibility of MRI-based reference images for image-guided radiotherapy of the pelvis with either cone-beam computed tomography or planar localization images," Acta Oncol. **54**(6), 889–895 (2015).
[9]J. Korhonen, "Magnetic resonance imaging -based radiation therapy—Methods enabling the radiation therapy treatment planning workflow for prostate cancer patients by relying solely on MRI-based images throughout the process," Doctoral dissertations, Aalto University Publication Series, 2015, Vol. 35, pp. 1–66, http://urn.fi/urn:isbn:978-952-60-6124-5.
[10]M. Kapanen and M. Tenhunen, "T1/T2*-weighted MRI provides clinically relevant pseudo-CT density data for the pelvic bones in MRI-only based radiotherapy treatment planning," Acta Oncol. **52**(3), 612–618 (2013).
[11]M. Kapanen, J. Collan, A. Beule, T. Seppala, K. Saarilahti, and M. Tenhunen, "Commissioning of MRI-only based treatment planning procedure for external beam radiotherapy of prostate," Magn. Reson. Med. **70**(1), 127–135 (2013).
[12]J. A. Dowling, J. Sun, P. Pichler, D. Rivest-Henault, S. Ghose, H. Richardson, C. Wratten, J. Martin, J. Arm, L. Best, S. S. Chandra, J. Fripp, F. W. Menk, and P. B. Greer, "Automatic substitute computed tomography generation and contouring for magnetic resonance imaging (MRI)-Alone external beam radiation therapy from standard MRI sequences," Int. J. Radiat. Oncol., Biol., Phys. **93**(5), 1144–1153 (2015).
[13]A. Johansson, M. Karlsson, and T. Nyholm, "CT substitute derived from MRI sequences with ultrashort echo time," Med. Phys. **38**(5), 2708–2714 (2011).
[14]J. M. Edmund, H. M. Kjer, K. Van Leemput, R. H. Hansen, J. A. Andersen, and D. Andreasen, "A voxel-based investigation for MRI only radiotherapy of the brain using ultra short echo times," Phys. Med. Biol. **59**(23), 7501–7519 (2014).
[15]T. Stanescu, H. S. Jans, N. Pervez, P. Stavrev, and B. G. Fallone, "A study on the magnetic resonance imaging (MRI)-based radiation treatment planning of intracranial lesions," Phys. Med. Biol. **53**(13), 3579–3593 (2008).
[16]S. H. Hsu, Y. Cao, K. Huang, M. Feng, and J. M. Balter, "Investigation of a method for generating synthetic CT models from MRI scans of the head and neck for radiation therapy," Phys. Med. Biol. **58**(23), 8419–8435 (2013).
[17]E. M. Kerkhof, J. M. Balter, K. Vineberg, and B. W. Raaymakers, "Treatment plan adaptation for MRI-guided radiotherapy using solely MRI data: A CT-based simulation study," Phys. Med. Biol. **55**(16), N433–N440 (2010).
[18]J. M. Edmund, D. Andreasen, F. Mahmood, and K. Van Leemput, "Cone beam computed tomography guided treatment delivery and planning verification for magnetic resonance imaging only radiotherapy of the brain," Acta Oncol. **54**(9), 1496–1500 (2015).
[19]M. S. Gudur, W. Hara, Q. T. Le, L. Wang, L. Xing, and R. Li, "A unifying probabilistic Bayesian approach to derive electron density from MRI for radiation therapy treatment planning," Phys. Med. Biol. **59**(21), 6595–6606 (2014).
[20]M. Karlsson, M. G. Karlsson, T. Nyholm, C. Amies, and B. Zackrisson, "Dedicated magnetic resonance imaging in the radiotherapy clinic," Int. J. Radiat. Oncol., Biol., Phys. **74**, 644–651 (2009).
[21]T. Bostel, N. H. Nicolay, J. G. Grossmann, A. Mohr, S. Delorme, G. Echner, P. Häring, J. Debus, and F. Sterzing, "MR-guidance—A clinical study to evaluate a shuttle- based MR-linac connection to provide MR-guided radiotherapy," Radiat. Oncol. **9**, 12 (8pp.) (2014).
[22]O. Green, S. Goddu, and S. Mutic, "Commissioning and quality assurance of the first commercial hybrid MRI-IMRT system," Med. Phys. **39**(6), 3785 (2012).
[23]T. Stanescu, T. Tadic, and D. A. Jaffray, "Commissioning of an MR-guided radiation therapy system," Int. J. Radiat. Oncol., Biol., Phys. **90**(1), 94–95 (2014).
[24]J. J. Lagendijk, B. W. Raaymakers, C. A. Van den Berg, M. A. Moerland, M. E. Philippens, and M. van Vulpen, "MR guidance in radiotherapy," Phys. Med. Biol. **59**(21), R349–R369 (2014).
[25]A. L. Appelt, J. Pløen, H. Harling, F. S. Jensen, L. H. Jensen, J. C. Jørgensen, J. Lindebjerg, S. R. Rafaelsen, and A. Jakobsen, "High dose chemoradiotherapy and watchful waiting for distal rectal cancer: A prospective observational study," Lancet Oncol. **16**(8), 919–927 (2015).
[26]A. C. Westphalen, D. A. McKenna, J. Kurhanewicz, and F. V. Coakley, "Role of magnetic resonance imaging and magnetic resonance spectroscopic imaging before and after radiotherapy for prostate cancer," J. Endourol. **22**(4), 789–794 (2008).
[27]T. J. Wallace, T. Torre, M. Grob, J. Yu, I. Avital, B. Brucher, A. Stojadinovic, and Y. G. Man, "Current approaches, challenges and future directions for monitoring treatment response in prostate cancer," J. Cancer **5**(1), 3–24 (2014).
[28]L. Sander, N. C. Langkilde, M. Holmberg, and J. Carl, "MRI target delineation may reduce long-term toxicity after prostate radiotherapy," Acta Oncol. **53**(6), 809–814 (2014).
[29]P. B. Romesser, O. Cahlon, E. Scher, Y. Zhou, S. L. Berry, A. Rybkin, K. M. Sine, S. Tang, E. J. Sherman, R. Wong, and N. Y. Lee, "Proton beam radiation therapy results in significantly reduced toxicity compared with intensity-modulated radiation therapy for head and neck tumors that require ipsilateral radiation," Radiother. Oncol. **118**, 286–292 (2016).

[30]P. W. McLaughlin, C. Evans, M. Feng, and V. Narayana, "Radiographic and anatomic basis for prostate contouring errors and methods to improve prostate contouring accuracy," Int. J. Radiat. Oncol., Biol., Phys. **76**(2), 369–378 (2010).
[31]B. W. Raaymakers, A. J. Raaijmakers, and J. J. Lagendijk, "Feasibility of MRI guided proton therapy: Magnetic field dose effects," Phys. Med. Biol. **53**(20), 5615–5622 (2008).
[32]R. D. Bucholz and D. D. Miller, "System combining proton beam irradiation and magnetic resonance imaging," U.S. Patent 6,725,078 (20 April 2004).
[33]C. M. Rank, N. Hunemohr, A. M. Nagel, M. C. Rothke, O. Jakel, and S. Greilich, "MRI-based simulation of treatment plans for ion radiotherapy in the brain region," Radiother. Oncol. **109**(3), 414–418 (2013).
[34]C. M. Rank, C. Tremmel, N. Hunemohr, A. M. Nagel, O. Jakel, and S. Greilich, "MRI-based treatment plan simulation and adaptation for ion radiotherapy using a classification-based approach," Radiat. Oncol. **8**, 51 (13pp.) (2013).
[35]J. Hartman, C. Kontaxis, G. H. Bol, S. J. Frank, J. J. W Lagendijk, M. van Vulpen, and B. W. Raaymakers, "Dosimetric feasibility of intensity modulated proton therapy in a transverse magnetic field of 1.5 T," Phys. Med. Biol. **60**(15), 5955–5969 (2015).
[36]J. Korhonen, M. Kapanen, J. Keyrilainen, T. Seppala, L. Tuomikoski, and M. Tenhunen, "Absorbed doses behind bones with MR image-based dose calculations for radiotherapy treatment planning," Med. Phys. **40**(1), 011701 (9pp.) (2013).
[37]M. D. Robson, P. D. Gatehouse, M. Bydder, and G. M. Bydder, "Magnetic resonance: An introduction to ultrashort TE (UTE) imaging," J. Comput. Assist. Tomogr. **27**(6), 825–846 (2003).
[38]H. Paganetti, "Range uncertainties in proton therapy and the role of Monte Carlo simulations," Phys. Med. Biol. **57**(11), 99–117 (2012).
[39]M. Urie, M. Goitein, W. R. Holley, and G. T. Chen, "Degradation of the Bragg peak due to inhomogeneities," Phys. Med. Biol. **31**(1), 1–15 (1986).
[40]W. Chen, Y. Liu, B. Guo, D. Jette, and N. Papanikolaou, "Boundary study of Bragg peak shift and Bragg peak degradation in proton dose calculation," Med. Phys. **36**(6), 2616 (2009).
[41]D. R. White, H. Q. Woodard, and S. M. Hammond, "Average soft tissue and bone models for use in radiation dosimetry," Br. J. Radiol. **60**(717), 907–913 (1987).
[42]H. Q. Woodard and D. R. White, "The composition of body tissues," Br. J. Radiol. **59**(708), 1209–1218 (1986).
[43]International Commission on Radiation Units and Measurements (ICRU), "Photon, electron, proton and neutron interaction data for body tissues," Report No. 46, Appendix A, ICRU, 1992, pp. 11–12, http://jicru.oxfordjournals.org.
[44]M. T. Torbey, M. Selim, J. Knorr, C. Bigelow, and L. Recht, "Quantitative analysis of the loss of distinction between gray and white matter in comatose patients after cardiac arrest," Stroke **31**(9), 2163–2167 (2000).
[45]Raysearch Laboratories, *Robust Optimization in Raystation* (RaySearch Laboratories AB, Sweden, Stockholm, 2015), white paper, version: 2015-08-05.
[46]A. J. Lomax, "Intensity modulated proton therapy and its sensitivity to treatment uncertainties 1: The potential effects of calculational uncertainties," Phys. Med. Biol. **53**(4), 1027–1042 (2008).
[47]A. J. Lomax, "Intensity modulated proton therapy and its sensitivity to treatment uncertainties 2: The potential effects of inter-fraction and inter-field motions," Phys. Med. Biol. **53**(4), 1043–1056 (2008).
[48]A. C. Kraan, S. van de Water, D. N. Teguh, A. Al-Mamgani, T. Madden, H. M. Kooy, B. J. Heijmen, and M. S. Hoogeman, "Dose uncertainties in IMPT for oropharyngeal cancer in the presence of anatomical, range, and setup errors," Int. J. Radiat. Oncol., Biol., Phys. **87**(5), 888–896 (2013).
[49]C. Siversson, F. Nordström, T. Nilsson, T. Nyholm, J. Jonsson, A. Gunnlaugsson, and L. E. Olsson, "Technical Note: MRI only prostate radiotherapy planning using the statistical decomposition algorithm," Med. Phys. **42**(10), 6090–6097 (2015).
[50]J. Kim, C. Glide-Hurst, A. Doemer, N. Wen, B. Movsas, and I. J. Chetty, "Implementation of a novel algorithm for generating synthetic CT images from magnetic resonance imaging data sets for prostate cancer radiation therapy," Int. J. Radiat. Oncol., Biol., Phys. **91**(1), 39–47 (2015).
[51]J. Unkelbach, T. C. Chan, and T. Bortfeld, "Accounting for range uncertainties in the optimization of intensity modulated proton therapy," Phys. Med. Biol. **52**(10), 2755–2773 (2007).
[52]M. Stuschke, A. Kaiser, J. Abu Jawad, C. Pottgen, S. Levegrun, and J. Farr, "Multi-scenario based robust intensity-modulated proton therapy (IMPT) plans can account for set-up errors more effectively in terms of normal tissue sparing than planning target volume (PTV) based intensity-modulated photon plans in the head and neck region," Radiat. Oncol. **8**, 145 (5pp.) (2013).
[53]M. Stuschke, A. Kaiser, C. Pottgen, W. Lubcke, and J. Farr, "Potentials of robust intensity modulated scanning proton plans for locally advanced lung cancer in comparison to intensity modulated photon plans," Radiother. Oncol. **104**(1), 45–51 (2012).
[54]A. Fredriksson, A. Forsgren, and B. Hardemark, "Minimax optimization for handling range and setup uncertainties in proton therapy," Med. Phys. **38**(3), 1672–1684 (2011).
[55]A. Fredriksson and R. Bokrantz, "A critical evaluation of worst case optimization methods for robust intensity-modulated proton therapy planning," Med. Phys. **41**(8), 081701 (11pp.) (2014).
[56]S. P. Crijns, B. W. Raaymakers, and J. J. Lagendijk, "Real-time correction of magnetic field inhomogeneity-induced image distortions for MRI-guided conventional and proton radiotherapy," Phys. Med. Biol. **56**(1), 289–297 (2011).
[57]K. L. Stephans, P. Xia, R. D. Tendulkar, and J. P. Ciezki, "The current status of image-guided external beam radiotherapy for prostate cancer," Curr. Opin. Urol. **20**(3), 223–228 (2010).
[58]S. Das, T. Liu, A. B. Jani, P. Rossi, J. Shelton, Z. Shi, and M. K. Khan, "Comparison of image-guided radiotherapy technologies for prostate cancer," Am. J. Clin. Oncol. **37**(6), 616–623 (2014).
[59]M. Yang, X. R. Zhu, P. C. Park, U. Titt, R. Mohan, G. Virshup, J. E. Clayton, and L. Dong, "Comprehensive analysis of proton range uncertainties related to patient stopping-power-ratio estimation using the stoichiometric calibration," Phys. Med. Biol. **57**(13), 4095–4115 (2012).
[60]A. Besemer, H. Paganetti, and B. Bednarz, "The clinical impact of uncertainties in the mean excitation energy of human tissues during proton therapy," Phys. Med. Biol. **58**(4), 887–902 (2013).
[61]M. Witt, U. Weber, D. Kellner, R. Engenhart-Cabillic, and K. Zink, "Optimization of the stopping-power-ratio to Hounsfield-value calibration curve in proton and heavy ion therapy," Z. Med. Phys. **25**(3), 251–263 (2015).